Climatic Controls on Metabolic Constraints in the Ocean

Precious Mongwe[1,2], Matthew Long[3], Takamitsu Ito[4,] Curtis Deutsch[5], and Yeray Santana-Falcón[6]

[1]Southern Ocean Carbon Climate Observatory (SOCCO), CSIR, Cape Town, South Africa

[2]National Institute for Theoretical and Computational Sciences (NITheCS), Cape Town, South Africa

[3]Oceanography Section, Climate and Global Dynamics Laboratory, National Center for Atmospheric Research, Boulder, CO, United States of America

[4]School of Earth and Atmospheric Sciences, Georgia Institute of Technology, Atlanta, Georgia United States of America

[5]Department of Geosciences, Princeton University, Princeton, NJ, United States of America

[6]CNRM, Université de Toulouse, Météo-France, CNRS, Toulouse, 31057, France

Corresponding Author: Precious Mongwe (pmongwe@csir.co.za)

Abstract

Observations and models indicate that climate warming is associated with the loss of dissolved oxygen from the ocean. Dissolved oxygen is a fundamental requirement for heterotrophic marine organisms (except marine mammals) and, since the basal metabolism of ectotherms increases with temperature, warming increases organisms' oxygen demand. Therefore, warming and deoxygenation pose a compound threat to marine ecosystems. In this study, we leverage an ecophysiological framework and compilation of empirical trait data quantifying the temperature sensitivity and oxygen requirements of metabolic rates for a range of marine species ("ecotypes"). Using the Community Earth System Model Large Ensemble, we investigate how natural climate variability and anthropogenic forcing impact the ability of marine environments to support aerobic metabolisms on interannual to multi-decadal timescales. Warming and deoxygenation projected over the next several decades will yield a reduction in the volume of viable ocean habitat. We find that fluctuations in temperature and oxygen associated with natural variability are distinct from those associated with anthropogenic forcing in the upper ocean. Further, the joint temperature-oxygen anthropogenic signal emerges sooner than temperature and oxygen independently from natural variability. Our results demonstrate that anthropogenic perturbations underway in the ocean will strongly exceed those associated with the natural system; in many regions, organisms will be pushed closer to or beyond their physiological limits, leaving the ecosystem more vulnerable to extreme temperature-oxygen events.

1. Introduction

Dissolved oxygen (O_2) is a fundamental metabolic requirement for heterotrophic marine organisms, excluding marine mammals (Portner, 2002; Keeling et al., 2010; Tiano et al., 2014). The decline ocean O_2 due to warming is a tendency long predicted by models (Keeling et al., 2010; Long et al., 2016; Oschlies et al., 2018) and recently found evident at the global scale in compilations of in situ observations (Schmidtko et al., 2017; Ito et al., 2017). Deoxygenation is driven by the direct effect of reduced oxygen solubility with warming compounded by buoyancy-induced stratification in the upper ocean, which weakens the ventilation-mediated supply of fresh oxygen to the ocean interior. While the full ecological implications of ocean deoxygenation remain uncertain, it is clear that the physiological impacts of oxygen loss on marine organisms can be considered explicitly in the context of warming: basal metabolic rates for ectothermic organisms depend on ambient temperature and increase with warming (Gillooly et al., 2001); thus, higher temperatures impose additional demand for oxygen to sustain aerobic respiration (Deutsch et al., 2015). Consequently, as the ocean warms, even present-day oxygen distributions may be insufficient to meet the oxygen demands of organisms living near key physiological thresholds (Deutsch et al., 2022).

Model projections clearly demonstrate that warming and deoxygenation are consequences of human-driven climate change, yet natural climate variability also produces important fluctuations in these quantities. Indeed, evidence suggests that natural variability contributes to hypoxic events, such as those observed in the California Current, where fish and benthic-organism mortality has been associated with low-O_2 waters impinging on the continental shelf (Pozo Buil and Di Lorenzo, 2017; Howard et al., 2020). A clear understanding of how natural climate variability drives fluctuations in metabolic state and the associated implications for organisms is a critical context in which to view long-term climate warming. Given that the natural system is highly dynamic, climate change signals are often masked by decadal-scale variability (Ito and Deutsch, 2010). While numerous authors have considered detection and attribution of climate change for physical and biogeochemical variables (Rodgers et al., 2015; Long et al., 2016; Schlunegger et al., 2019), comparatively little attention has been devoted to explicitly characterizing the relative influence of natural and anthropogenic drivers of changes in the ocean's capacity to support aerobic life. In this study, we approach this challenge by

leveraging the concept of the Metabolic Index (Φ) introduced by Deutsch et al. (2015). Φ is based on the notion that aerobic organisms can persist only where the ambient oxygen partial pressure (pO_2) is sufficient to sustain respiration. Φ incorporates an explicit representation of the dependence of metabolic oxygen demand on temperature, thus providing a framework to consider how joint oxygen and temperature variability constrain viable habitat in the ocean.

Many ocean organisms may already be under threat from deoxygenation (Hoegh-Guldberg and Bruno, 2010; Breitburg et al., 2018); however, ongoing climate-driven loss of oxygen raises important questions about the future of marine ecosystems: How will anthropogenic changes in dissolved oxygen and temperature affect the capacity of ocean habitats to support aerobic metabolism? What is the spatial and temporal distribution of changes in the ocean's metabolic state associated with climate variability? At what point can anthropogenic change in the ocean's metabolic state be distinguished from natural variability? This study addresses these questions using a combination of metabolic theory, a dataset quantifying key physiological parameters for a collection of marine species adapted to specific environments ("ecotypes"), and the oxygen and temperature distributions as simulated in the Community Earth System Model, version 1 Large Ensemble (CESM1-LE), which includes 34 members simulating ocean biogeochemistry under climate variability and change from 1920–2100 forced using historical data and the Representative Concentration Pathway Scenario 8.5 (RCP85) (Kay et al., 2015; Long et al., 2016).

This paper is organized as follows. Section 2 presents a brief overview of the relevant metabolic theory, the associated empirical datasets, and describes our approach to analysis. In Section 3 we present results quantifying the joint temperature-oxygen variability simulated in the CESM1-LE, evaluating the spatiotemporal structure of variability in marine ecotype habitat, including long-term trends based on the RCP8.5 scenario and time of emergence (ToE). The main outcomes of the results are synthesized in Section 4 and summarized in Section 5.

2. Datasets and methods

2.1 Metabolic index

Empirical studies measuring thermal tolerance and oxygen requirements in the laboratory on an array of marine organisms have enabled an assessment of lethal thresholds (Vaquer-Sunyer and Duarte, 2008; Rosewarne et al., 2016). These data coupled with recent advances in a theoretical framework enable both explanatory and predictive power in the context of a dynamic environment (Deutsch et al., 2015; Penn et al., 2018; Howard et al., 2020). The fundamental insights here are that basal metabolic rates for ectothermic marine organisms depend on ambient temperature and generally increase with warming (Gillooly et al., 2001). Increasing basal metabolic rates impose additional demand for oxygen. Organisms use oxygen dissolved in seawater and acquisition tends to be limited by diffusive processes; thus, oxygen supply is related to the ambient pO_2. The ratio of oxygen supply to temperature-dependent demand provides a critical indicator of the capacity for an organism to meet its metabolic requirements. Deutsch et al. (2015) formalized these concepts into a quantity termed the "Metabolic Index (Φ)", which is defined as the ratio of oxygen supply to an organism's resting metabolic demand. Oxygen supply is parameterized according to a biomass-dependent scaling of pO_2, capturing variation in the efficiency with which organisms acquire and utilize O_2. This can be expressed as $S = \hat{\alpha}_s \, B^{\sigma} pO_2$, where $\hat{\alpha}_s$ represent gas transfer between an organism and its environment and B^{δ} is the scaling of supply with biomass, B (Piiper et al., 1971). Gas supply is represented as an Arrhenius function;

$$\hat{\alpha}_s = \alpha_s exp\{\frac{-E_s}{K_B}\left[\frac{1}{T} - \frac{1}{T_{ref}}\right]\} \quad (1)$$

Resting metabolic demand is also expressed using the Arrhenius equation as

$$D = \alpha_D B^{\delta} exp\{\frac{-E_d}{K_B}\left[\frac{1}{T} - \frac{1}{T_{ref}}\right]\}, \quad (2)$$

where α_D is a species-specific basal metabolic rate, E_d (eV) is the temperature dependence of oxygen supply, T is temperature, T_{ref} is the reference temperature (15°C), and k_B is the Boltzmann constant (Gillooly et al., 2001). Gas transfer is kinematically slow at low temperatures, and hence organism viability can be limited by the energy to acquire oxygen at low temperatures, thus E_o varies with temperature. Here we account for this by adding the temperature dependence (dE_o/dT) to E_o in equations above ($E_o + \frac{dE_o}{dT}(T - T_{ref})$), using the mean

value of dE_o/dT = 0.022 eV consistent with Deutsch et al. (2020). The Metabolic Index can thus be written as the ratio of *S/D*:

$$\Phi = \frac{\alpha_s}{\alpha_D}\frac{B^{\sigma}}{B^{\delta}}\, pO_2 exp\{\frac{-E_s}{K_B}\left[\frac{1}{T}-\frac{1}{T_{ref}}\right]+\frac{E_d}{K_B}\left[\frac{1}{T}-\frac{1}{T_{ref}}\right]\},$$

$$= A_o B^{\sigma-\delta} pO_2 exp\{\frac{E_d-E_s}{K_B}\left[\frac{1}{T}-\frac{1}{T_{ref}}\right]\},$$

$$= A_o pO_2 exp\{\frac{E_o}{K_B}\left[\frac{1}{T}-\frac{1}{T_{ref}}\right]\}, \quad (3)$$

where $A_o = \alpha_S/\alpha_D$ *(1/atm)* is the hypoxic tolerance, $E_o = E_d - E_s$ (E_s is the temperature dependence of oxygen supply) (Deutsch et al., 2015; Penn et al., 2018). The exponent, $\varepsilon = \sigma - \delta$, is the allometric scaling of the supply to demand ratio with biomass, is typically near zero. Therefore, in the analysis that follows, we presume unit biomass and thus neglect potential impacts of variations in biomass.

If Φ falls below a critical threshold value of 1, conditions are physiologically unsustainable: an organism cannot meet its basic resting metabolic oxygen requirements. Conversely, values of Φ above 1 enable organismal metabolic rates to increase by a factor of Φ above resting levels, permitting critical activities such as feeding, defence, growth, and reproduction. Thus, for a given environment and species, Φ provides an estimate of the ratio of maximum sustainable metabolic rate to the minimum rate necessary for basal metabolism. Deutsch et al. (2015) inferred the ratio of active to resting energetic demand by examining the biogeographic distribution of several species, finding that range boundaries coincide with values of Φ = 1.5–7. This threshold, termed critical rate (Φ_{crit}), represents the minimum metabolic index required for an organism to sustain an active metabolic state, which is a more meaningful ecological threshold than requirements for resting metabolism. Therefore, in this study, we define a quantity Φ' derived by dividing Φ by Φ_{crit}, so when Φ falls below 1, the organism can no longer sustain its active metabolic demand and will need to make physiological trade-offs. Accounting for these active metabolic requirements, we use an adjusted definition of the hypoxic tolerance trait, $A_c = A_o / \Phi_{crit}$, where A_c is termed the "ecological hypoxia tolerance", consistent with Howard et al., 2020. Where $\Phi' > 1$ (i.e., $\Phi > \Phi_{crit}$) an organism can sustain an active metabolic rate; where $\Phi' < 1$ (i.e., $\Phi < \Phi_{crit}$), O_2 is insufficient and an active metabolic state is not viable. Henceforth, our

149 analysis focuses on Φ'; in the subsequent metabatic index refers to Φ' (Φ' = Φ) throughout the
150 text and figures.
151
152 **2.2 Physiological dataset**
153 We make use of a dataset describing physiological parameters for a collection of 61 marine
154 ecotypes spanning a range of ecological hypoxic tolerances (A_c) and temperature sensitivities
155 (E_o) (Penn et al., 2018; Deutsch et al., 2020, Figure 1a). The 61 species span benthic and pelagic
156 habitats across four phyla in all ocean basins (Arthropoda, Chordata, Mollusca, and Cnidaria).
157 The dataset include 28 malacostracans, 21 fishes, three bivalves and cephalopods, two copepods,
158 and one each for gastropods, ascidians, scleractinian corals, and sharks with body mass spans of
159 eight orders of magnitude (Penn et al., 2018). We illustrate how the physiological traits E_o and A_c
160 constrain habitat viability in the context of distributions of pO_2 and temperature in the marine
161 environment in Figure 1b, which shows the minimum pO_2 (i.e., pO_2 at Φ_{crit}) required to sustain
162 an active metabolic state as a function of temperature for five combinations of E_o and A_c. The
163 five combinations are derived from sampling the probability distributions of E_o and A_c (Figure
164 1a) at the 10^{th}, 50^{th}, and 90^{th} percentile values (illustrated by colored stars in Figure 1a and
165 corresponding curves in Figure 1b). We assume that the trait distributions are independent, which
166 is a reasonably modest simplification; E_o is represented by a normal distribution and A_c by a
167 lognormal distribution function (Figure S1). The pO_2 at Φ_{crit} curves shown in Figure 1b delineate
168 regions of pO_2-temperature space that are habitable (above the curve) and uninhabitable (below
169 the curve). The reversing curvature of pO_2 at Φ_{crit} in Figure 1b at low temperature captures the
170 decrease of the organism's oxygen acquisition efficiency in cooler conditions yielding cold
171 intolerance. At very low temperatures, gas transfer is limited by the decrease in molecular gas
172 diffusion, as a consequence, oxygen transfer into the organisms requires energy, yielding cold

intolerance, this is well illustrating by the blue line in Figure 1b.

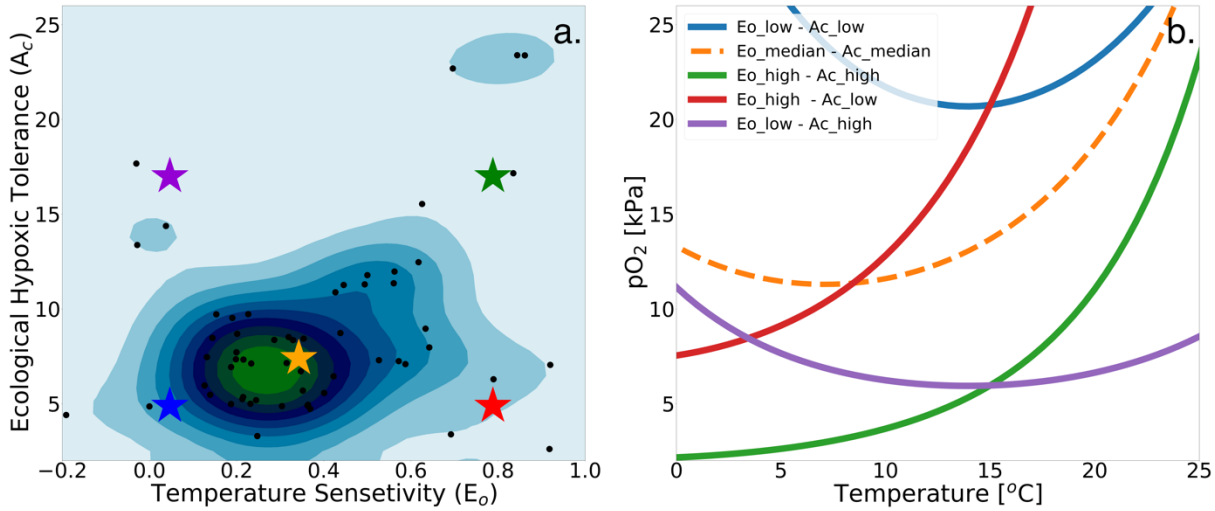

Figure 1. Physiological traits determining hypoxic tolerance. (a) Scatter plot of 61 marine ecotypes for which empirically derived estimates of activation energy (E_o) and the ecological hypoxic tolerance (A_c) have been determined (Penn et al., 2018). The color shows the density of occurrence for the 61 marine ecotypes in the A_c - E_o trait space. (b) The minimum pO_2 required to sustain an active metabolic state (i.e., pO_2 at Φ_{crit}, Deutsch et al., 2020) for five combinations of A_c and E_o corresponding to the stars in panel "a"; these are combinations of the 10th, 50th, 90th percentile values for each parameter. Below the pO_2 lines shown, the organism would experience an oxygen deficit relative to its active metabolism requirements, effectively signifying the species-specific hypoxic conditions, based on physiological traits, for this range of temperatures.

To illustrate how the trait combinations of E_o and A_c exert control on the geographic distribution of organisms in the marine environment (Deutsch et al., 2020), we use observations of pO_2 and T along a zonal transect of the Pacific Ocean and plot Φ' for nine combinations of E_o and A_c percentile values (Figure 2). The colorbar in Figures 2a-i show the metabolic index for an active state (Φ'); regions with values above one are habitable (color), while regions with values below one are uninhabitable (white) on the basis of metabolic constraints (other ecological considerations are not considered). The subplots in the upper portion of the figure are arranged according to the same trait axes shown in Figure 1a; E_o increases horizontally from left to right and A_c increases from the bottom to the top. For the trait combination in the bottom left (low E_o, low A_c; Figure 2g), metabolism is relatively insensitive to temperature, and tolerance for low pO_2 is poor. Thus, ecotypes with low E_o and low A_c are restricted to high latitude surface waters, where temperatures are cool, and pO_2 is abundant (Figure 2g). As E_o increases from left to right,

metabolic rates become more sensitive to temperature. Then, habitat is gained at depth, where temperatures are cooler and higher temperature sensitivity confers an advantage (Figure 2g–i). From the bottom to the top, the increase in tolerance of low pO_2 conditions increases habitability in regions of low pO_2, enabling organisms to expand beyond high-latitude surface waters (Figure 2g-a). The biogeographic range for organisms with high A_c is modulated by E_o; as temperature sensitivity increases, ecotype viability at high latitudes is increased, but tropical surface waters become less viable (Figure 2 a-c). Henceforth, our analysis will utilize the metabolic index of the median ecotype (E_o = 0.34, A_c= 7.4; Figure 2e) for illustrative purposes; i.e., all metabolic index figures refer to this median ecotype unless otherwise stated.

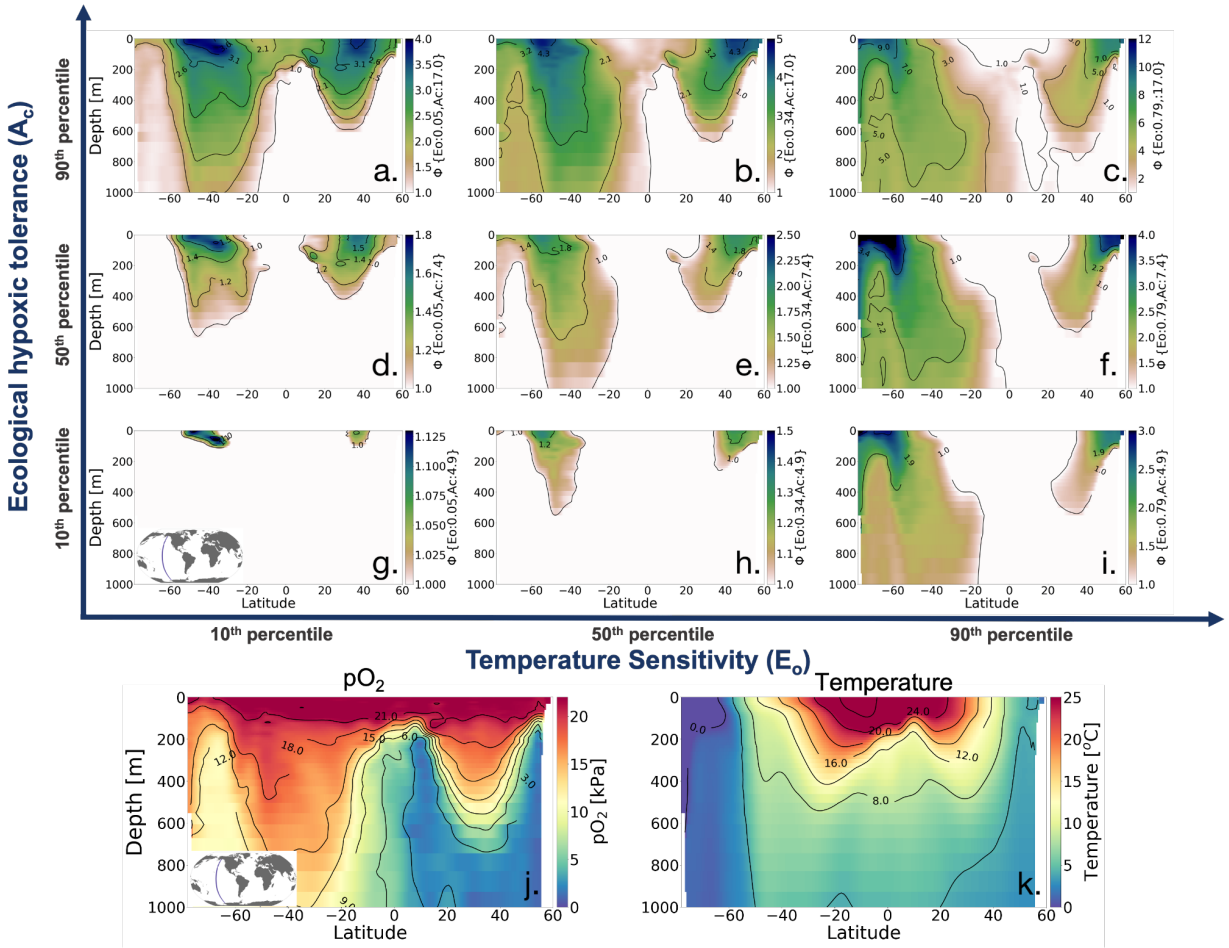

Figure 2. Annual mean metabolic index (Φ') for nine combinations of the ecological traits E_o (metabolic temperature sensitivity) and A_c (ecological hypoxic tolerance) along a transect in the Pacific Ocean based on a climatology from the World Ocean Atlas dataset (Garcia et al., 2014). The percentile values of each trait are: 10th (E_o = 0.04, A_c= 4.8), 50th (E_o = 0.34, A_c= 7.4), and 90th (E_o = 0.79, A_c= 17.0). The lower panels show pO_2 and

temperature from the WOA dataset. Note that the colorbar range differs by panel and values where $\Phi' < 1$ are omitted, thus the color shows only areas where an active metabolic state can be sustained.

2.3 Earth system model simulations

This study is based on the CESM1-LE, described in detail by Kay et al. (2015). The CESM1-LE included 34 ensemble members integrated from 1920–2100 under historical and RCP8.5 forcing. The ensemble was generated by adding round-off level (10^{-14} K) perturbations to the air temperature field at initialization in 1920; this small difference yields rapidly diverging model solutions due to the chaotic dynamics intrinsic to the climate system, thus developing ensemble spread representative of internal variability (Kay et al., 2015). Briefly, the CESM1-LE uses the Community Earth System Model, version 1 (Hurrell et al., 2013), with a horizontal resolution of nominally 1° in all components. The ocean component is Parallel Ocean Program version 2, (Smith et al., 2010) with sea ice simulated by the Los Alamos Sea Ice Model version 4 (Hunke and Lipscomb, 2010). Ocean biogeochemistry was represented by the Biogeochemical Elemental Cycling (BEC) model (Moore et al., 2013; Lindsay et al., 2014).

Our analysis focuses on three depths: 50 m representing near-surface dynamics, the epipelagic zone at 200 m, and the mesopelagic zone at 500 m. pO_2 was calculated using the Garcia and Gordon. (1992) solubility formulation. For convenience, we use the period 1920–1965 to define a minimally-perturbed natural state, as this period is prior to the development of substantial anthropogenic trends in ocean oxygen and temperature (Long et al., 2016). We also examine distributions over the last three decades of the 21st century (2070–2099) to evaluate the projected climate-change signal under RCP8.5. We use the mean across all 34 ensemble members to quantify the deterministic, "forced" response of the climate system to anthropogenic influence (Deser et al., 2012). The ensemble spread is thus indicative of the amplitude of variations attributable to natural variability.

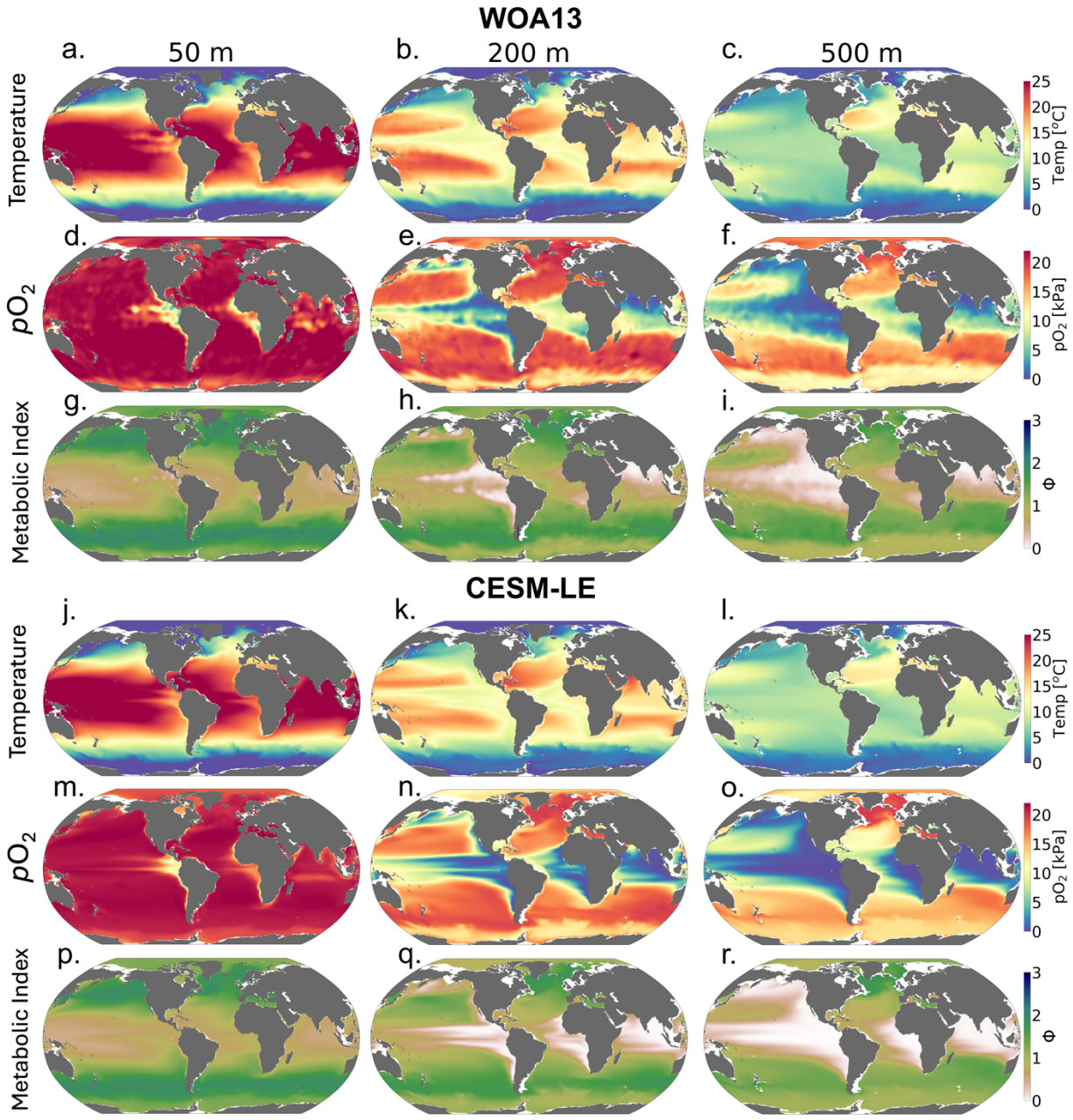

Figure 3. Mean-state comparison with observations. The climatological mean of (top rows) temperature (°C), (middle rows) pO_2 (kPa), and the (bottom rows) metabolic index for active metabolism (Φ') for the median ecotype (E_o = 0.34, A_c= 7.4); three depths are shown (left) 50 m, (center) 200 m, and (right) 500. Top panels show the WOA13 dataset and the bottom panels show CESM1-LE.

We compared the CESM1-LE (1920 - 1965) with the World Ocean Atlas, version 2013 (WOA2013) dataset (Garcia et al., 2014), an observationally-based, gridded climatology (Figure

245 3a-i). CESM1-LE generally provides a reasonable representation of pO_2 and temperature
246 distributions at the selected depths (Figure 3); however, there are important biases to
247 acknowledge in the context of interpreting the results. Temperature magnitudes are generally
248 well simulated in the CESM1-LE, showing a root mean square error (RMSE) < 1.3 °C, and
249 pattern correlation coefficient (PCC) >0.98 in all three selected depths (50 m, 200 m, and 500)
250 (Table 1). Temperature magnitudes are slightly underestimated at 50 m and 200 m (mean bias of
251 < 0.3°C), and overestimated by 0.41 °C at 500 m. Note that since our comparison uses CESM1-
252 LE data from 1920-1965, some discrepancy in temperature might be expected from the signal of
253 climate warming present in the WOA observations. pO_2 is also reasonably well captured by the
254 CESM1-LE (PCC <0.95), but magnitudes are slightly underestimated at depth, showing a mean
255 bias of -1.63 kPa and -2.1 kPa at 200 m and 500 m with respect to WOA13 (Table 1). Regions of
256 low pO_2 waters are too extensive in CESM1-LE (Figure 3n-o) and there is a slight degradation of
257 skill with depth for pO_2 fields (Table 1). The underestimation of pO_2 leads to a slight
258 underestimation of Φ' with respect to WOA13, and overestimate habitat loss in the future
259 climate (Figure 3 p-r); however, Φ' computed from the model fields demonstrates that the
260 dominant spatial patterns are well captured by the CESM1-LE despite magnitudes that are
261 slightly too low (i.e., Figure 1, c, l). This CESM pO_2 bias is common among coarse-resolutions
262 ocean models and it is attributed to a sluggish circulation and hence weak ventilation (Long et
263 al., 2016). These differences ultimately matter most near the hypoxic zones and at the boundaries
264 of habitable zones like the Oxygen Minimum Zones (OMZs).
265
266

Table 1. Summary statistics for the comparison of CESM1-LE with the World Ocean Atlas dataset (Garcia et al., 2014). The columns include the mean bias, pattern correlation coefficient (PCC), and root mean square error (RMSE) at 50 m, 200 m, and 500 m.

	Mean bias	**R**	**RMSE**
	Temperature [°C]		
50 m	-0.17	0.99	1.22
200 m	-0.25	0.99	1.22
500 m	0.10	0.98	0.63
	pO_2 [kPa]		
50 m	0.05	0.99	1.91
200 m	-1.17	0.96	5.96
500 m	-1.46	0.95	6.28
	Metabolic index		
50 m	0.01	0.99	0.02
200 m	-0.09	0.97	0.05
500 m	-0.15	0.96	0.08

2. Results

3.1 Joint temperature-pO_2 natural variability and forced trends

The spatial distribution of the number of viable ecotypes is shown in Figure 4 for the "unperturbed" climate (1920-1965). Our intention here is not to quantify the actual biogeographic range of organisms in the environment, but rather to illustrate the ocean's ability to support respiration by marine ectotherms given the metabolic capacities afforded within the trait space of extant organisms. High latitude environments do not impose strong aerobic constraints (cold intolerance notwithstanding), thus over much of the Southern Ocean, North Atlantic, and Arctic Ocean almost all 61 ecotypes can sustain respiration. The tropical oceans impose the strongest aerobic constraints, restricting the viability of ecotypes that do not have high-hypoxia tolerance (A_o). For example, less than 25 ecotypes are viable over much of the tropical surface ocean (Figure 4a); low concentrations of oxygen at depth impose even stronger constraints, and no ecotypes are viable in the core of OMZs (Figure 4b, c). The spatial patterns of the number of viable ecotypes is tightly controlled by temperature at the surface, since pO_2 is mostly near saturated levels; at depth, however, pO_2 is the dominant driver of geographic patterns in ecotype viability (Figures 2-4). Temperature generally decreases with depth, reducing the metabolic oxygen demand. However, since pO_2 also decreases with depth and displays greater lateral heterogeneity, pO_2 emerges as the dominant constraint of spatial structure in ecotype viability at depth.

The standard deviation of annual anomalies using all CESM1-LE ensemble members provides insight into the amplitude of natural variability (Figure. 5, one standard deviation). Temperature and pO_2 show similar patterns of natural variability in the upper ocean, both showing particularly large variance in the western tropical Pacific and Indian Ocean (Figure 5 a, d). Spatial variation in the magnitude of temperature variability generally decreases with depth, but pO_2 displays even relatively larger variability at depth with respect to the surface in some regions (Figure 5 a–f). The joint pO_2-temperature variability manifests in variations of Φ' (Figure 5g-i). Natural variability in Φ' computed for the median ecotype shows spatial patterns similar to temperature

in the upper-surface ocean (50 m), but is more similar to pO_2 at depth. Thus, variations in Φ' tend to be temperature-dominated near the surface, but are more strongly controlled by pO_2 variability at depth. Φ' also shows the most extensive natural variability at 200 m consistent with the variability of pO_2. The number of viable species shows more dramatic fluctuations than variations in the median ecotype Φ'; variations in the number of viable ecotypes exceed 30% on annual timescales in the tropical upper ocean and near OMZ boundaries in the water column (Figure 4 c–d). This reflects the fact that interannual variability can preclude habitability for some regions of the A_c-E_o trait space, but these variations do not necessarily impact viability for the median ecotype (Figure 1). In the tropical surface ocean, high temperatures (>25ºC), and saturated surface (pO_2 >20 kPa) require high hypoxia tolerance (A_c), but permit a range of E_o values (Figure 1b, 2a-b). Ecotypes with larger temperature sensitivity (high E_o) are particularly responsive to variations in temperature.

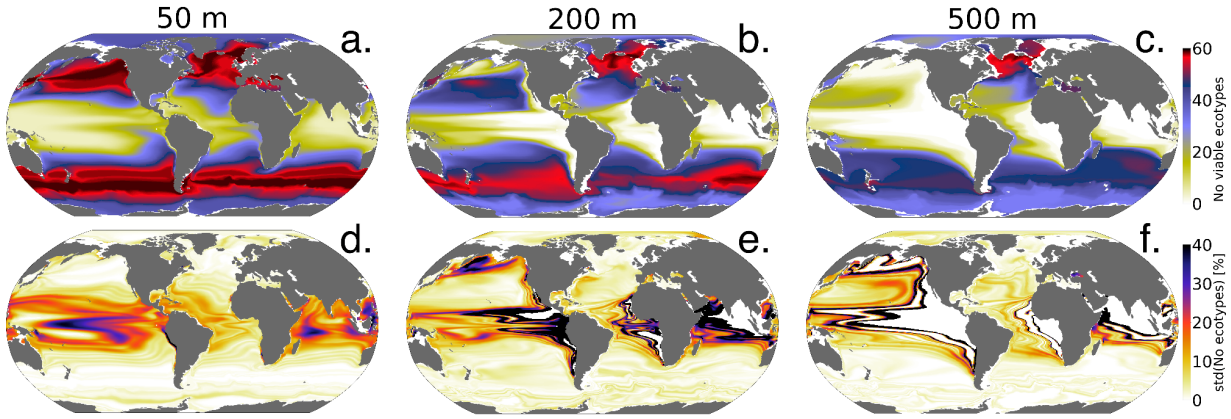

Figure 4. Metabolic constraints on trait-space viability. Top row: the number of ecotypes from the physiological trait database that are viable (total = 61) in the CESM1-LE over the period 1920–1965. Bottom row: the standard deviation (expressed as a percent of the mean) in the number of viable ecotypes, reflecting fluctuations driven by natural variability.

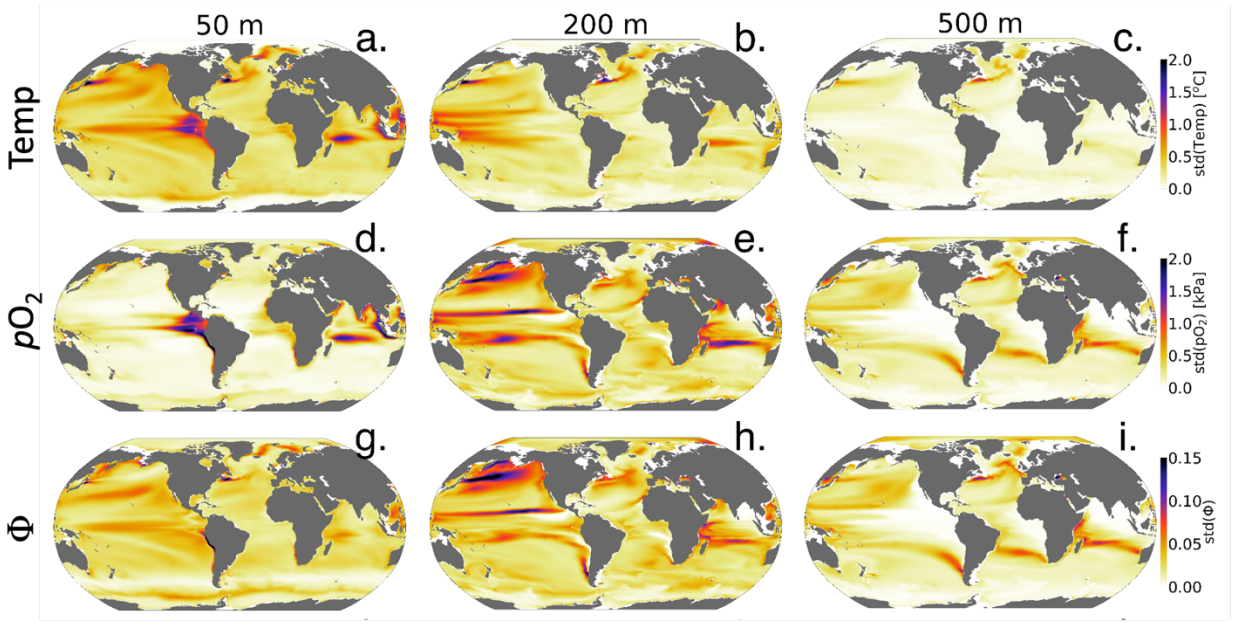

Figure 5. The amplitude of natural variability in the ocean's metabolic state. The panels show the standard deviation of annual-mean anomalies of all ensemble members over the period 1920–1965 for (top row) temperature (°C), (middle row) pO_2 (kPa), and (bottom row) the metabolic index (unitless) of the median ecotype (E_o = 0.34, A_c= 7.4).

CESM1-LE simulates nearly homogeneous warming between 1920–1965 and 2070–2099 in the surface ocean (50 m) under RCP8.5, with an exception of the so-called North Atlantic warming hole (Figure 6a). Both modelling and observational studies have linked the North Atlantic warming hole to the slowing of the Atlantic overturning circulation with climate change (Keil et al., 2020). The magnitude of ocean warming generally diminishes with depth except in the North Atlantic, where, despite reductions, the overturning circulation effectively propagates anthropogenic heat anomalies into the ocean interior. pO_2 shows heterogeneous changes between 1920–1965 and 2070–2099 (Figure 6 d-f). In the upper ocean, pO_2 changes are generally small (< 1 kPa) because the near-surface is kept close to saturation via photosynthetic oxygen production and air-sea equilibration. At depth, however, pO_2 shows long-term changes linked to accumulated effects of respiration and changes in circulation (Ito et al., 2017). At 200 m for example, the Pacific Ocean displays a basin-wide mean reduction in pO_2 of 2 kPa (~30%), while the Atlantic and Indian basins gain about >2 kPa (~ 10 - 35%) by the end of the century. The largest long-term pO_2 loss (>3 kPa) occurs in the North Pacific while the largest pO_2 gain (~2

kPa) occurs in the North Atlantic gyre and western Indian Ocean (Figure 6 e-f).

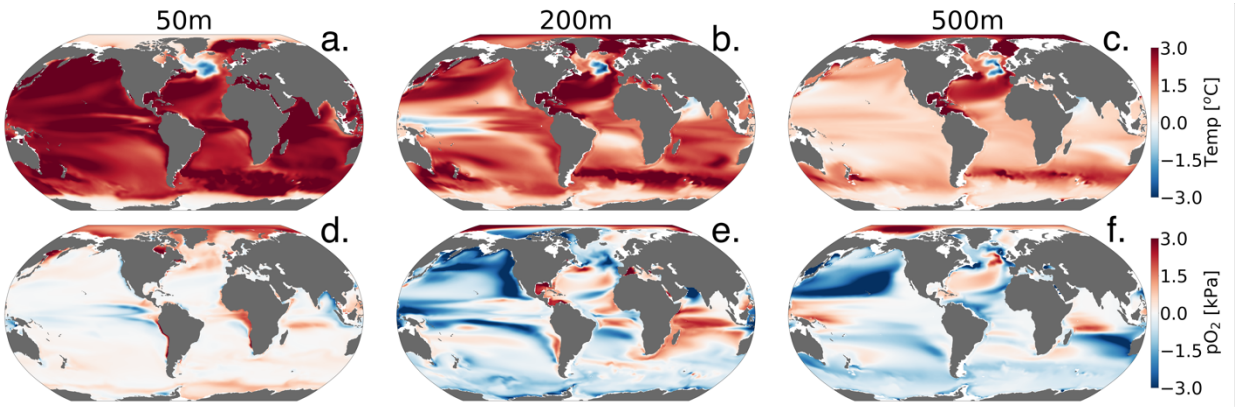

Figure 6. Net long-term change (2070–2099 minus 1920–1965) in the CESM1-LE ensemble means temperature (top) and (bottom) pO_2 at 50 m, 200 m, and 500 m.

Figure 7 shows the relationship between interannual variations in pO_2 versus temperature (pO_2-T) in the unperturbed climate (1920–1965; top row) and for the forced trend associated with 21st century climate change (2070–2099 minus 1920–1965; bottom row). The nature of the pO_2-T relationship is an important indicator of the impacts of variability on the metabolic state. Furthermore, the extent to which the forced trend is characterized by a pO_2-T relationship that is distinct from that associated with natural variability provides insight into the potential for advanced or delayed detection of signals in Φ relative to pO_2 or temperature alone. Given that metabolic rates for most organisms increase with temperature (positive E_o), a positive correlation between variations in temperature and pO_2 is generally indicative of compensating changes, wherein increased oxygen demand is at least partially offset by increased supply. Anticorrelation between temperature and pO_2, by contrast, will generally be associated with compounding impacts on the metabolic index, as a negative correlation indicates that reductions in pO_2 (i.e., oxygen supply) accompany warming (i.e., increased demand). The sign of the pO_2-T relationship in the natural climate varies regionally and with depth (Figure 7, top row). The surface ocean is generally characterized by a weak, positive pO_2-T relationship, which could manifest from, among other mechanisms, temperature-induced increases in photosynthetic oxygen production (Figure 7a). The natural pO_2-T relationship in the epipelagic (200 m) is characterized by strong positive correlations in the tropics and negative correlations at high latitudes (Figure 7b). A positive correlation between pO_2 and temperature at this depth could be induced by variability

associated with adiabatic vertical displacement of isopycnals, or “heave”, which has the effect of translating background gradients in properties vertically in the water column (Long et al., 2016). Upward movement of a deep isopycnal surface would yield a negative temperature anomaly and a negative pO_2 anomaly (positive correlation), as the deeper, colder waters have greater oxygen utilization signatures associated with longer ventilation age. Negative correlations between pO_2 and temperature could manifest from ventilation processes, where enhanced subduction of surface water yields anomalously cold water masses that are enriched in oxygen. The sign of these epipelagic pO_2-T correlations shows some similarity to those associated with the externally forced climate (Figure 6e), but the latter is characterized by a greater prevalence of anticorrelation, most notably in the North Pacific ocean. At 500 m depth, the relationship between temperature and pO_2 in the natural climate is almost a mirror image of the epipelagic (Figure 7c); the tropics generally display negative correlations, while polar regions show positive correlations (Figure 7 e). The pO_2-T relationship in the forced trend at 500 m is dominated by broad regions of deeply negative correlations, with the most pronounced effect again in the North Pacific. The negative relationship is consistent with a ventilation signal, as buoyancy-induced stratification from warming curtails the introduction of new oxygen into the ocean interior. The predominantly negative pO_2-T relationship associated with the forced trend is indicative of the compounding effects of climate change on metabolic state, increasing metabolic demand while simultaneously reducing oxygen supply.

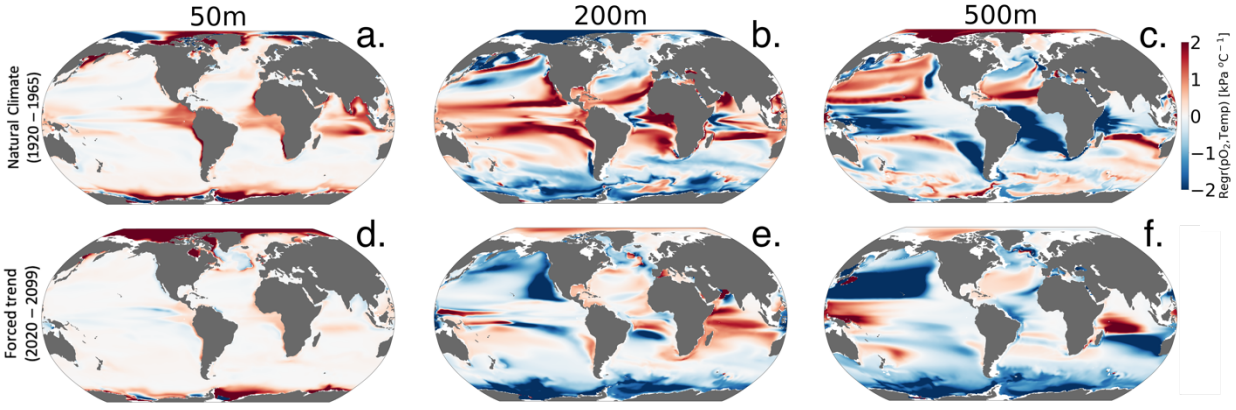

Figure 7. Regression of annual means pO_2 versus temperature (kPa $^{o}C^{-1}$) for (top row) interannual variability and (bottom row) the forced trend (difference between 2020–2099 and 1920–1965). The columns show the regressions computed at different depths, 50 m, 200 m, and 500 m, respectively.

3.2 Long-term habitat changes

Figure 8 shows the climate-driven changes in Φ' for the median ecotype, as well as the impacts of climate change on the number of viable ecotypes. Notably, while pO_2 in the near-surface ocean is relatively insensitive to climate change (Figure 6d), there are reductions in Φ' in the tropics (Figure 9d), owing to the direct impacts of warming. These changes are associated with deep reductions in the number of viable ecotypes in the tropics (Figure 8a). There are modest increases in Φ' and ecotype viability at high-latitudes; metabolic state in these regions is affected by cold intolerance, thus warming broadens the viable region of trait space. Additionally, sea ice melt support an increase in pO_2, as gas exchange becomes more effective at restoring equilibrium oxygen concentrations. The number of viable ecotypes shows more intense patterns than those in the median ecotype Φ' in the upper ocean (Figure 8). This is partly because ecotypes predicted to lose viability in the tropical regions (~ 50%) are at the extremes of the A_c-E_o distribution (Figure 1) and not captured by the median ecotype Φ'. Nevertheless, outside the tropical regions, the median ecotype gives a good indication of the anthropogenic impact to marine ectotherms. The projected habitat loss in the epipelagic-pelagic North Pacific (> 50%) and habitat gain in the epipelagic-pelagic Southern Indian Ocean (~40%) and pelagic western tropical regions (~40%) are consistent with a decrease in the median ecotype Φ'. Note that the most pronounced effects on habitat are associated with regions where climate change drives a strongly negative pO_2-temperature relationship (Figure 7).

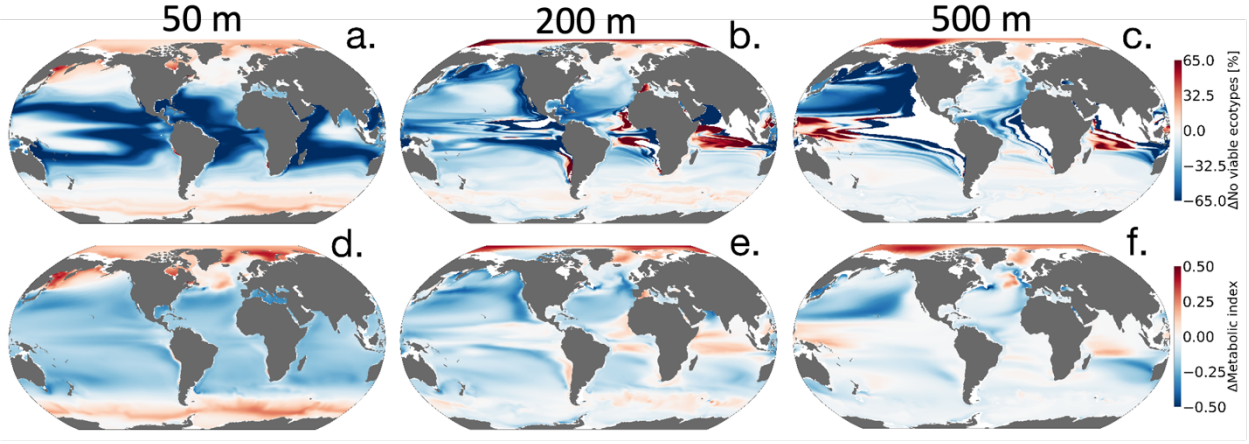

Figure 8. Net change in the number of habitable ecotypes in percentage (top row). Net metabolic index change

(2070 - 2099 vs. 1920 - 1965) for the median ecotype [E_o = 0.34, A_c= 7.4] (bottom row). At 50m (first column), 200m (second column) and 500m (third column).

3.3 Time of Emergence

In this section, we examine the "time of emergence" (ToE, Hawkins and Sutton, 2012), the point when forced changes in pO_2, temperature and Φ' can be distinguished from the background natural variability. We define ToE as the time when the magnitude of change in the ensemble mean of a particular variable exceeds two standard deviations of the natural climate (1920 - 1965). This is illustrated in Figure 9 for a single grid point in the North Pacific at 200 m. At this location, the forced trend in temperature shows a monotonic increase, while pO_2 shows a monotonic decrease; as a result, Φ' for the median ecotype and the number of viable ecotypes decrease over time. The anti-correlation between pO_2 and temperature exacerbates trends in Φ', and hence the forced trend of the median ecotype Φ' emerges from natural noise earlier than either pO_2 or temperature do alone (Figure 10a-c). Note that although the ToE of ecotype viability change is directly derived from changes in Φ', it is binary counted; changes in ecotype viability are counted in whole numbers and this creates a step-function temporal-spatial variation (Figure 9d). Consequently, this step-function-like feature of ecotype viability creates discontinuities even in spatial patterns of ToE (Figure 10 j-l) as also shown in the natural variance in Figure 4 d-f.

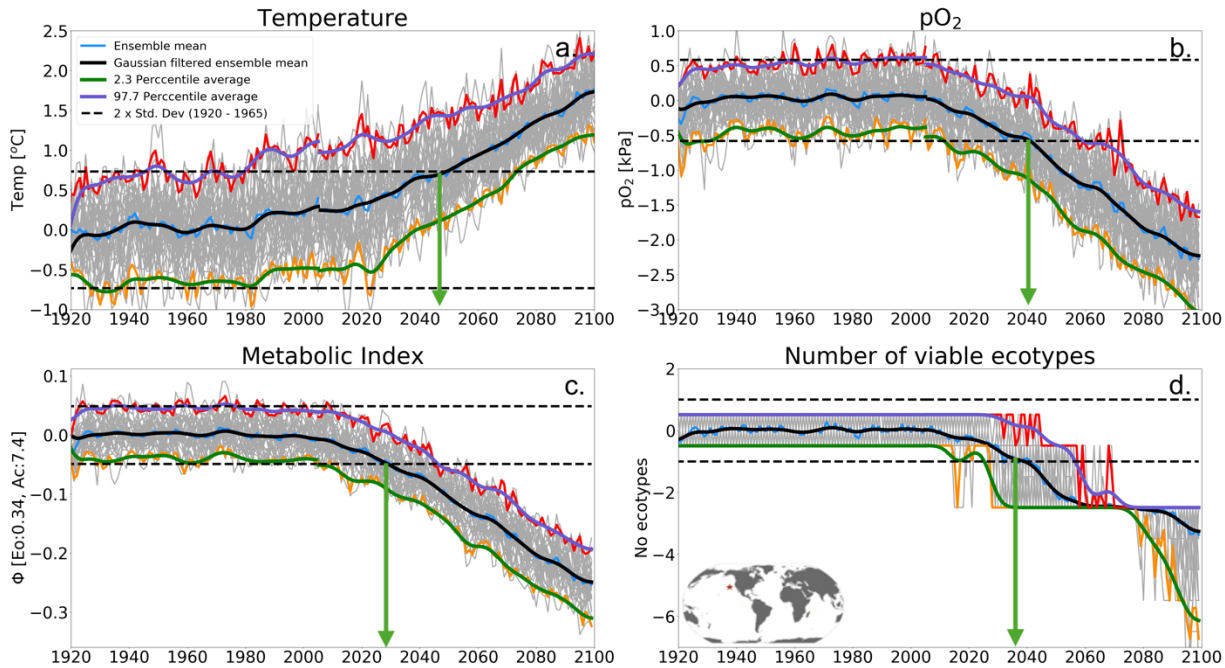

Figure 9.. Time of emergence (ToE) of the climate forcing signal for (a) temperature, (b) pO_2 (c) the metabolic index of the median ecotype [E_o = 0.34, A_c= 7.4], and (d) the number of viable ecotypes for a single model grid in the North Pacific at 200 m. ToE (green arrows) is defined as the time when the forced trend signal (ensemble member time series) is above two standard deviations (black dotted line) of all ensemble members for the period 1920 - 1965.

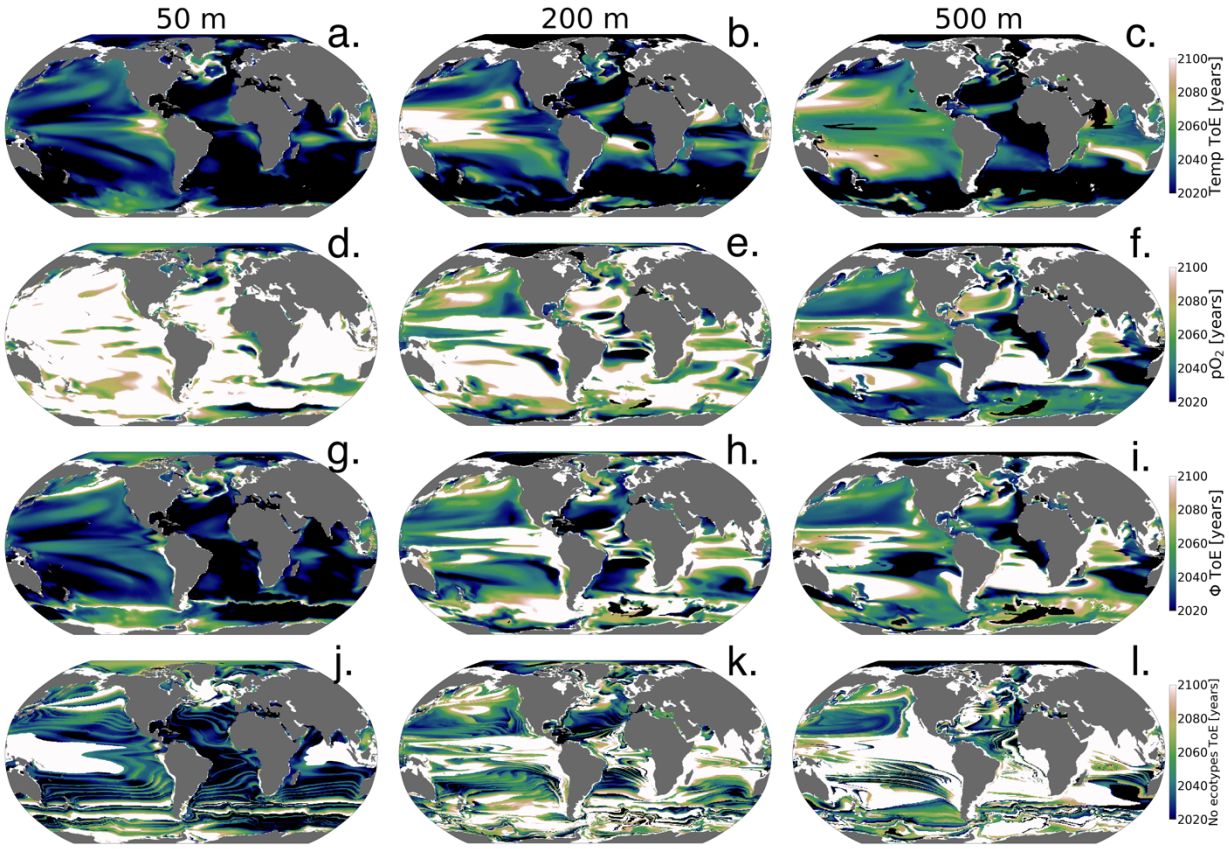

Figure 10. Time of emergence (ToE) of the climate forcing signal for temperature, pO_2, phi, and the number of viable ecotypes. ToE is defined as the time when the forced trend signal (ensemble member time series) is above two standard deviations of all ensemble members for the period 1920 - 1965.

The ToE of pO_2 and temperature are inverted with depth; temperature emerges earliest in the upper ocean while pO_2 emerges earlier at depth and later or shows no emergence in the upper ocean (Figure 10 a-f). This feature is consistent with larger upper ocean temperatures long-term changes and greater pO_2 changes at depth. Near-surface ocean temperature has mostly already emerged by 2020 and is predicted to have almost completely emerged by the late 2060s under RCP85 (Figure 10 a-c). The early emergence of temperature from natural noise also persists for regions of relatively low natural variance at depth, e.g., the Southern Ocean and Atlantic Basin Gyres. Regions of the largest natural variability (see Figure 5) like the subtropical-subpolar Pacific however do not emerge until close to the end of the century. For pO_2, anthropogenic changes in the upper ocean generally do not emerge from natural noise before the end of the century except for the Arctic Ocean and Eastern Antarctic. In the Arctic Ocean and Eastern

Antarctic pO_2 gain is related to sea-melt emergence by the mid-2050s (Figure 10a). The median ecotype Φ' ToE shows spatial patterns that are coherent with temperature ToE in the upper ocean with exception of polar regions. In contrast, they are consistent with pO_2 ToE patterns at depth; this is consistent with net long-term Φ' changes in Figure 9d. The emergence of the anthropogenic signal in ecotype viability closely resembles the median ecotype Φ' spatial patterns but showing non-harmonious spatial patterns due to the step-function-like counting feature of viability changes. It shows that the predicted ~ 50% ecotype viability loss in the tropics (Figure 6a) may already be distinguishable from natural variability by the mid-2030s. In the North Pacific, the predicted > 50% ecotype viability loss in the epipelagic-pelagic regions is predicted to start emerging in the 2040s at 500 m and 2080s at 200 m (Figure 10 k-l).

In summary, we showed that because of the surface ocean's large warming signal and the least pO_2 loss outside of the polar regions under the RCP85 climate scenario, it is characterized by habitat loss in the tropics and a slight habitat gain in polar regions (Figure 11). Sea-ice melts support Oxygen gain through the enhancement of temperature-driven solubility in the surface polar regions. At depth, warming is less prevalent by the end of the 21st century; however, oxygen loss related to the weakening ventilation of the ocean interior as the ocean becomes more stratified has a stronger impact on metabolic reliance, leading to habitat loss in tropics and subtropics. On the other hand, cooler temperatures and efficient ventilation in polar regions create an oxygen-rich environment. Thus, in contrast to tropical and subtropical regions, warming leads to a slight habitat gain (Figure 11), as organisms escape the cold intolerance imposed by molecular gas diffusion at low temperatures.

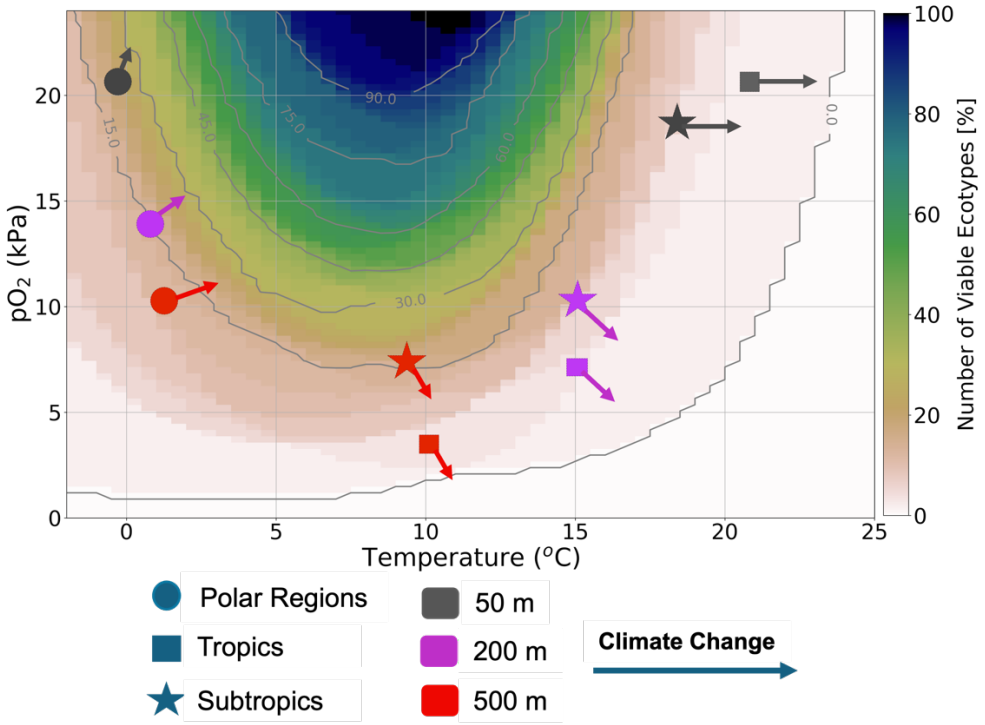

Figure 11. Summary Figure: It shows the distribution of ecotype viability within representative ocean temperature and pO_2 boundaries for the 66 species analysed in this study. The markers represent the subsampled regions, with polar regions denoted by circles, tropical regions by squares, and subtropical regions by stars. The colours represent the depth levels; 50 m (grey), 200 m (purple), and 500 m (red). Each arrow shows the estimated joint temperature-pO_2 climate change vector based on the net changes in temperature and pO_2 (as depicted in Figure 6).

4. Discussion

The human-induced rapid warming of the planet has been shown to drive ocean deoxygenation (Ito et al., 2017; Schmidtko et al., 2017; Long et al., 2016). Higher metabolic oxygen demand at higher temperatures (Gillooly et al., 2001; Deutsch et al., 2015, 2022) raises concerns about the ability of marine ectotherms to support aerobic respiration in the future. This study set out to characterize the anticipated climate change signal in the ocean's metabolic state in the context of natural variability using the metabolic theory as a basis to examine the capacity of the environment to support ectothermic marine heterotrophs.

493 The spatial variation in pO_2 and temperature in the unperturbed natural climate state set
494 biogeographic boundaries based on ectotherms' physiological performance. The resilience of
495 these ectotherms' biogeographic structure to natural variability and long-term climate warming is
496 perturbed by the joint pO_2-temperature changes, effectively measured by the metabolic index
497 (Φ'). An increase in the capacity of the organisms to support aerobic respiration increases Φ'; for
498 example by ocean cooling or increase in oxygen supply contrary, warming and decrease in
499 oxygen supply decrease Φ'. There are exceptions in extremely low-temperature environments
500 (Figure 11), where aerobic respiration is also limited by kinematic gas transfer into the organism
501 in addition to environmental oxygen supply. Relative changes in pO_2 and temperature in the
502 natural variability and forced trend, therefore, regulate ectotherms' resilience to environmental
503 changes. Under the RCP85 climate scenario, the ocean generally warms homogeneously but
504 concurrent pO_2 changes are heterogeneous and vary with depth. Thus, the characteristics of these
505 pO_2-temperature forced trend changes determine when the climate change impact on marine
506 ectotherms can be distinguishable from natural variability.
507
508 In the surface ocean, pO_2 is generally abundant and relatively uniform, and thus spatial
509 temperature variations have a dominant constraint on the spatial variations of organismic
510 metabolic state. The warmest parts of the surface ocean, the tropical oceans, can only support
511 about 10-20 (~ 30%) of the 61 ecotypes while cooler regions in the extra tropics have nearly
512 100% viability. Moreover, since warming anomalies propagate from the surface, the surface
513 tropical oceans also show the largest natural variance in temperature and ecotype viability. This
514 is because extremely warm temperatures in the surface tropics (>25^{o}C) are mainly suited for
515 organisms with high-temperature sensitivity (E_o), which are relatively fewer, and mostly close to
516 their physiological limits (Storch et al., 2014). Large natural variability in these warmest parts of
517 the tropical surface ocean precludes the forced trend signal from emerging from the natural
518 variability in the ecotype viability by end of the century although the ocean warms the largest in
519 the surface. Nevertheless, the large warming trends in the surface ocean generally emerge
520 relatively early (the 2020s) from natural variability in both temperature and ecotype viability in
521 most regions. Minimal changes in surface pO_2 in the forced trend affirm that surface ocean
522 marine ectotherms are mainly perturbed by temperature in the context of anthropogenic changes.
523 In polar regions, warming has a counterintuitive effect on marine ectotherms with respect to

most parts of the surface ocean. There, warming helps organisms escape extreme cold intolerances by enhancing membrane kinematic gas transfer which enhances Φ' and thus ecotype richness in the future (Figure 11)

In the epipelagic and mesopelagic regions (200 m and 500 m), the forced temperature trend and natural variability are broadly smaller than the surface ocean, while pO_2 changes show the opposite. Thus, at depth pO_2 play a more intricate role in perturbating marine ectotherm habitats in the context of anthropogenic warming with respect to the surface ocean, where temperature plays a dominant role. Contrasting the regression between pO_2 and temperature in the natural climate, and forced trends provides an instructive framework to analysing ectotherms' long-term changes. Regions showing different correlations between temperature and pO_2 in the forced trends in comparison to the natural climate suggest a loss of metabolic resilience; loss of habitat, and these regions tend to have a relatively early ToE. For instance, in the epipelagic and mesopelagic North Pacific, temperature-pO_2 regressions switched from a positive correlation in the unperturbed climate to a strong negative correlation in the forced trend (Figure 7). The North Pacific pelagic – epipelagic regions is projected to lose nearly half of the present climate ecotype viability by end of the 21st century, the projected habitat loss start emerging by the late 2030s under the RCP85 climate scenario, On the other hand, in the Arctic Ocean and some parts of the Southern Ocean, same sign pO_2-temperature correlations in the forced trends result in the preservation of the marine habitat and even slight enhancements.

5. Conclusions

The joint temperature-oxygen metabolic framework in this study provides additional insight into the impact of climate change on marine ecosystems in comparison to the independent oxygen or temperature analysis. We here showed that while warming is the leading order driving mechanism of climate change, the direct effect of warming on marine ecosystems is mostly in the upper ocean. Climate change-related oxygen loss is a major driver of marine ecosystem stress in addition to warming at depth. Incorporating organismal physiological sensitivity to oxygen-temperature changes in the metabolic framework provides insight into how climate impacts the

biogeographic structure of marine habitat. We find that forced perturbations to pO_2 and temperature will strongly exceed those associated with the natural system in many parts of the upper ocean, mostly pushing organisms in these environments closer to or beyond their physiological limits. Climate warming is expected to drive significant marine habitat loss in the surface tropical oceans and epipelagic - pelagic North Pacific Basin, while gaining marginal habitat viability in the surface Arctic Ocean and some parts of the Ocean Southern.

6. Competing interests

The contact author has declared that none of the authors has any competing interests

7. Acknowledgments

PM, ML, CD and TI were funded by the National Science Foundation (NSF) grant agreement No. 1737158. PM and YSF were also funded by the European Union's Horizon 2020 research and innovation programme under grant agreement No. 820989 (COMFORT).). We also would like to acknowledge the data access and computing support provided by the NCAR Cheyenne HPC.

8. Author contribution

PM and ML designed the study approach. PM developed the analysis with feedback from ML, CD and TI. PM prepared the manuscript with contributions from all co-authors.

9. Data access

The CESM1 large ensemble data used in this study can be accessed in this location: https://www.cesm.ucar.edu/community-projects/lens/data-sets

10. References

583 Breitburg, D., Levin, L. A., Oschlies, A., Grégoire, M., Chavez, F. P., Conley, D. J., Garçon, V.,
584 Gilbert, D., Gutiérrez, D., Isensee, K., Jacinto, G. S., Limburg, K. E., Montes, I., Naqvi, S. W.
585 A., Pitcher, G. C., Rabalais, N. N., Roman, M. R., Rose, K. A., Seibel, B. A., Telszewski, M.,
586 Yasuhara, M., and Zhang, J.: Declining oxygen in the global ocean and coastal waters,
587 https://doi.org/10.1126/science.aam7240, 5 January 2018.
588
589 Deser, C., Phillips, A., Bourdette, V., and Teng, H.: Uncertainty in climate change projections:
590 The role of internal variability, Clim Dyn, 38, 527–546, https://doi.org/10.1007/s00382-010-
591 0977-x, 2012.
592
593 Deutsch, C., Ferrel, A., Seibel, B., Pörtner, H. O., and Huey, R. B.: Climate change tightens a
594 metabolic constraint on marine habitats, Science (1979), 348, 1132–1135,
595 https://doi.org/10.1126/science.aaa1605, 2015.
596
597 Deutsch, C., Penn, J. L., and Seibel, B.: Metabolic trait diversity shapes marine biogeography,
598 Nature, 585, 557–562, https://doi.org/10.1038/s41586-020-2721-y, 2020.
599
600 Deutsch, C., Penn, J. L., Verberk, W. C. E. P., Inomura, K., Endress, M.-G., and Payne, J. L.:
601 Impact of warming on aquatic body sizes explained by metabolic scaling from microbes to
602 macrofauna, https://doi.org/10.1073/pnas, 2022.
603
604 Garcia, H. E. and Gordon, L. I.: Oxygen solubility in seawater: Better fitting equations,
605 https://doi.org/10.4319/lo.1992.37.6.1307, 1992.
606
607 Garcia, H. E. , Boyer, T. P. , Locarnini, R. A. , Antonov, J. I. , Mishonov, A. V. , Baranova, O.
608 K. , Melissa, M. Z. , Reagan, J. R. , and Johnson, D. R. ,: WORLD OCEAN ATLAS 2013
609 Volume 3: Dissolved Oxygen, Apparent Oxygen Utilization, and Oxygen Saturation, 75,
610 https://doi.org/10.7289/V5XG9P2W, 2014.
611
612 Gillooly, J., Brown, J., West, G., Savage, V., Charnov, E., Gillooly, J. F., Brown, J. H., West, G.
613 B., Savage, V. M., and Charnov, E. L.: Effects of size and temperature on metabolic rate
614 Recommended Citation, 2001.
615
616 Hawkins, E. and Sutton, R.: Time of emergence of climate signals, Geophys Res Lett, 39,
617 https://doi.org/10.1029/2011GL050087, 2012.
618
619 Hoegh-Guldberg, O. and Bruno, J. F.: The Impact of Climate Change on the World's Marine
620 Ecosystems, New Series, 328, 1523–1528, https://doi.org/10.1126/science.ll85779, 2010.

Howard, E. M., Penn, J. L., Frenzel, H., Seibel, B. A., Bianchi, D., Renault, L., Kessouri, F., Sutula, M. A., Mcwilliams, J. C., and Deutsch, C.: Climate-driven aerobic habitat loss in the California Current System, 2020.

Hunke, E. C. and Lipscomb, W. H.: CICE: the Los Alamos Sea Ice Model Documentation and Software User's Manual Version 4.1 LA-CC-06-012, 2010.

Hurrell, J. W., Holland, M. M., Gent, P. R., Ghan, S., Kay, J. E., Kushner, P. J., Lamarque, J. F., Large, W. G., Lawrence, D., Lindsay, K., Lipscomb, W. H., Long, M. C., Mahowald, N., Marsh, D. R., Neale, R. B., Rasch, P., Vavrus, S., Vertenstein, M., Bader, D., Collins, W. D., Hack, J. J., Kiehl, J., and Marshall, S.: The community earth system model: A framework for collaborative research, Bull Am Meteorol Soc, 94, 1339–1360, https://doi.org/10.1175/BAMS-D-12-00121.1, 2013.

Ito, T. and Deutsch, C.: A conceptual model for the temporal spectrum of oceanic oxygen variability, Geophys Res Lett, 37, https://doi.org/10.1029/2009GL041595, 2010.

Ito, T., Minobe, S., Long, M. C., and Deutsch, C.: Upper ocean O2 trends: 1958–2015, Geophys Res Lett, 44, 4214–4223, https://doi.org/10.1002/2017GL073613, 2017.

Kay, J. E., Deser, C., Phillips, A., Mai, A., Hannay, C., Strand, G., Arblaster, J. M., Bates, S. C., Danabasoglu, G., Edwards, J., Holland, M., Kushner, P., Lamarque, J. F., Lawrence, D., Lindsay, K., Middleton, A., Munoz, E., Neale, R., Oleson, K., Polvani, L., and Vertenstein, M.: The community earth system model (CESM) large ensemble project : A community resource for studying climate change in the presence of internal climate variability, Bull Am Meteorol Soc, 96, 1333–1349, https://doi.org/10.1175/BAMS-D-13-00255.1, 2015.

Keeling, R. F., Körtzinger, A., and Gruber, N.: Ocean deoxygenation in a warming world, Ann Rev Mar Sci, 2, 199–229, https://doi.org/10.1146/annurev.marine.010908.163855, 2010.
Keil, P., Mauritsen, T., Jungclaus, J., Hedemann, C., Olonscheck, D., and Ghosh, R.: Multiple drivers of the North Atlantic warming hole, Nat Clim Chang, 10, 667–671, https://doi.org/10.1038/s41558-020-0819-8, 2020.

Lindsay, K., Bonan, G. B., Doney, S. C., Hoffman, F. M., Lawrence, D. M., Long, M. C., Mahowald, N. M., Moore, J. K., Randerson, J. T., and Thornton, P. E.: Preindustrial-control and twentieth-century carbon cycle experiments with the Earth system model CESM1(BGC), J Clim, 27, 8981–9005, https://doi.org/10.1175/JCLI-D-12-00565.1, 2014.

Long, M. C., Deutsch, C., and Ito, T.: Finding forced trends in oceanic oxygen, Global Biogeochem Cycles, 30, 381–397, https://doi.org/10.1002/2015GB005310, 2016.

Moore, J. K., Lindsay, K., Doney, S. C., Long, M. C., and Misumi, K.: Marine ecosystem dynamics and biogeochemical cycling in the community earth system model [CESM1(BGC)]: Comparison of the 1990s with the 2090s under the RCP4.5 and RCP8.5 scenarios, J Clim, 26, 9291–9312, https://doi.org/10.1175/JCLI-D-12-00566.1, 2013.

Oschlies, A., Brandt, P., Stramma, L., and Schmidtko, S.: Drivers and mechanisms of ocean deoxygenation, https://doi.org/10.1038/s41561-018-0152-2, 1 July 2018.

Penn, J. L., Deutsch, C., Payne, J. L., and Sperling, E. A.: Temperature-dependent hypoxia explains biogeography and severity of end-Permian marine mass extinction, Science (1979), 362, https://doi.org/10.1126/science.aat1327, 2018.

Piiper, J., Dejours', P., Haab, P., and Rahn, H.: CONCEPTS AND BASIC QUANTITIES IN GAS EXCHANGE PHYSIOLOGY, Respiration Physiology, 292–304 pp., 1971.

Portner, H. O.: Climate variations and the physiological basis of temperature dependent biogeography: systemic to molecular hierarchy of thermal tolerance in animals, Comparative Biochemistry and Physiology Part A, 739–761 pp., 2002.

Pozo Buil, M. and Di Lorenzo, E.: Decadal dynamics and predictability of oxygen and subsurface tracers in the California Current System, Geophys Res Lett, 44, 4204–4213, https://doi.org/10.1002/2017GL072931, 2017.

Rodgers, K. B., Lin, J., and Frölicher, T. L.: Emergence of multiple ocean ecosystem drivers in a large ensemble suite with an Earth system model, Biogeosciences, 12, 3301–3320, https://doi.org/10.5194/bg-12-3301-2015, 2015.

Rosewarne, P. J., Wilson, J. M., and Svendsen, J. C.: Measuring maximum and standard metabolic rates using intermittent-flow respirometry: A student laboratory investigation of aerobic metabolic scope and environmental hypoxia in aquatic breathers, J Fish Biol, 88, 265–283, https://doi.org/10.1111/jfb.12795, 2016.

Schlunegger, S., Rodgers, K. B., Sarmiento, J. L., Frölicher, T. L., Dunne, J. P., Ishii, M., and Slater, R.: Emergence of anthropogenic signals in the ocean carbon cycle, Nat Clim Chang, 9, 719–725, https://doi.org/10.1038/s41558-019-0553-2, 2019.

Schmidtko, S., Stramma, L., and Visbeck, M.: Decline in global oceanic oxygen content during the past five decades, Nature, 542, 335–339, https://doi.org/10.1038/nature21399, 2017.

Smith, R., Jones, P., Briegleb, B., Bryan, F., Danabasoglu, G., Dennis, J., Dukowicz, J., Eden, C., Fox-Kemper, B., Gent, P., Hecht, M., Jayne, S., Jochum, M., Large, W., Lindsay, K.,

Maltrud, M., Norton, N., Peacock, S., Vertenstein, M., and Yeager, S.: The Parallel Ocean Program (POP) Reference Manual Ocean Component of the Community Climate System Model (CCSM) and Community Earth System Model (CESM) 1, 2010.

Storch, D., Menzel, L., Frickenhaus, S., and Pörtner, H. O.: Climate sensitivity across marine domains of life: Limits to evolutionary adaptation shape species interactions, Glob Chang Biol, 20, 3059–3067, https://doi.org/10.1111/gcb.12645, 2014.

Tiano, L., Garcia-Robledo, E., Dalsgaard, T., Devol, A. H., Ward, B. B., Ulloa, O., Canfield, D. E., and Peter Revsbech, N.: Oxygen distribution and aerobic respiration in the north and south eastern tropical Pacific oxygen minimum zones, Deep Sea Res 1 Oceanogr Res Pap, 94, 173–183, https://doi.org/10.1016/j.dsr.2014.10.001, 2014.

Vaquer-Sunyer, R. and Duarte, C. M.: Thresholds of hypoxia for marine biodiversity, 2008.